Intel Serv Robotics (2010) 3:163–173
DOI 10.1007/s11370-010-0067-2

ORIGINAL RESEARCH PAPER

A non-iterative and effective procedure for simultaneous odometry and camera calibration for a differential drive mobile robot based on the singular value decomposition

Gianluca Antonelli · Fabrizio Caccavale · Flavio Grossi · Alessandro Marino

Received: 3 April 2010 / Accepted: 12 May 2010 / Published online: 3 June 2010

Abstract Differential-drive mobile robots are usually equipped with video cameras for navigation purposes. In order to ensure proper operational capabilities of such systems, several calibration steps are required to estimate the video-camera intrinsic and extrinsic parameters, the relative pose between the camera and the vehicle frame and the odometric parameters of the vehicle. In this paper, simultaneous estimation of the aforementioned quantities is achieved by a novel and effective calibration procedure. The proposed calibration procedure needs only a proper set of landmarks, on-board measurements given by the wheels encoders, and the camera (i.e., a number of properly taken camera snapshots of the set of landmarks). A major advantage of the proposed technique is that the robot is not required to follow a specific path: the vehicle is asked to roughly move around the landmarks and acquire at least three snapshots at some approximatively known configurations. Moreover, since the whole calibration procedure does not use external measurement devices, it can be used to calibrate, on-site, a team of mobile robots with respect to the same inertial frame, given by the position of the landmarks' tool. Finally, the proposed algorithm is systematic and does not require any iterative step. Numerical simulations and experimental results, obtained by using a mobile robot Khepera III equipped with a low-cost camera, confirm the effectiveness of the proposed technique.

Keywords Camera calibration · Odometry calibration · Mobile robots

G. Antonelli · F. Grossi
Dipartimento di Automazione, Elettromagnetismo, Ingegneria dell'Informazione e Matematica Industriale, Università degli Studi di Cassino, Via G. Di Biasio 43, 03043 Cassino (FR), Italy
e-mail: antonelli@unicas.it

F. Caccavale · A. Marino (✉)
Dipartimento di Ingegneria e Fisica dell'Ambiente, Università degli Studi della Basilicata, Viale dell'Ateneo Lucano 10, 85100 Potenza, Italy
e-mail: alessandro.marino@unibas.it

F. Caccavale
e-mail: fabrizio.caccavale@unibas.it

1 Introduction

Differential-drive mobile robots equipped with a video-camera need careful calibration before the robot device is operational: namely, odometry, the video-camera and the relative vehicle-camera pose (hand-eye) calibration.

Odometry is the reconstruction of the mobile robot configuration (i.e., position and orientation) by resorting to encoders' measurements at the wheels. Starting from a known configuration, the current position and orientation of the robot is obtained by time integration of the vehicle's velocity corresponding to the measured wheels' velocity.

Video-camera calibration concerns both intrinsic parameters (e.g., the focal length) and extrinsic parameters (e.g., the relative pose of the image frame with respect to an inertial frame). This relatively mature topic is widely tackled in the literature (see, e.g., [9] for wide overview of existing calibration techniques).

When a camera is mounted on a robot, an additional calibration procedure is required: namely, the so-called hand-eye calibration [18], which is aimed at determining the relative pose between the camera and a robot-fixed frame. Although its name is inherited from the specific problem of a camera mounted on the end-effector of a robot manipulator, this step is, of course, required for a camera mounted on a mobile

robot as well. In general, such a calibration is required for any kind of sensors mounted on a robotic device.

Several research efforts have been focused on the aforementioned calibration problems, although they have been tackled individually; e.g., for odometry calibration, external video cameras (already calibrated) have been used, while hand-eye calibration is usually achieved by resorting to kinematically calibrated robots. In detail, as for the odometry calibration, since the first attempts [19], there has been an intense research activity aimed at improving the accuracy and the effectiveness of the calibration. A widely adopted algorithm is presented in [3], where the sole odometry calibration is object of study. In [6], an algorithm, based on the boundedness property of the error for Generalized-Voronoi-Graph-based paths, has been proposed and experimentally validated. In [7], it is proposed to drive the robot through a known path and then evaluate the shape of the resulting path to estimate the unknown parameters. The works [14,15] present a method to identify two systematic and two non-systematic errors, while in [11,12], the error propagation in vehicle odometry is analytically discussed, and two main results are given, namely, regarding the quadratic dependency of the estimation error with respect to the traveled distance and the existence of path-independent systematic errors. In [2], a calibration method aimed at identifying a 4-parameter odometric model has been proposed, where the linear relation between the unknowns and the measurements allows to use linear estimation tools; this linear estimation approach is further improved in [1] so as to estimate the physical odometric parameters, thus yielding a 3-parameter model. It is worth noticing that all the aforementioned methods require external measurement systems such as, e.g., calibrated video cameras or ranging sensors. Recently, in [4] simultaneous calibration of odometry and range sensors is achieved by resorting to on-board sensors only; the considered range sensor is a laser range finder assumed to be perfectly horizontal (i.e., the problem is planar).

In this paper simultaneous calibration of the intrinsic and extrinsic video-camera parameters, hand-eye, and odometry is achieved by resorting to a novel and effective procedure. The proposed calibration procedure needs a *landmarks tool*, i.e., a tool on which a set of geometric landmarks has been placed; the landmark tool is used to define the inertial reference frame as well. In addition to measurements given by the on-board camera, only measurements given by the wheel encoders are required. In detail, the video-camera is used to save a number of properly taken snapshots of the landmarks tool taken from different locations. A major advantage of the proposed technique is that no specific path is required to be followed: the vehicle is asked to roughly move around the landmarks and acquire a minimum of three snapshots at some approximatively known configurations. Moreover, since the whole calibration procedure does not use external measurement devices, it can be used to calibrate a team of mobile robots (performing, e.g., a search-and-rescue operation) with respect to the same inertial frame, given by the position of the landmarks tool. Finally, the proposed algorithm is systematic and does not require any iterative step. Numerical simulations and experimental results, obtained by using a Khepera III mobile robot equipped with a low-cost camera, confirm the effectiveness of the proposed technique.

Table 1 Definition of the main variables

$\Sigma_o - \{\boldsymbol{O}_o, \boldsymbol{x}_o, \boldsymbol{y}_o, z_o\}$	Inertial frame
$\Sigma_v - \{\boldsymbol{O}_v, \boldsymbol{x}_v, \boldsymbol{y}_v, z_v\}$	Vehicle-fixed frame
$\Sigma_c - \{\boldsymbol{O}_c, \boldsymbol{x}_c, \boldsymbol{y}_c, z_c\}$	Camera-fixed frame
x, y, θ	Vehicle configuration
v, ω	Vehicle linear/angular velocities
ω_R, ω_L	Right/left wheel angular velocities
θ_R, θ_L	Right/left wheel angular position
r_R, r_L, b	Right/left wheel radii, wheelbase
α_R, α_L	Intermediate odometric variables
$\boldsymbol{R}_r(\theta)$	Rotation matrix representing a rotation of θ around the $\boldsymbol{r}$ axis
$\boldsymbol{R}_a^b \in \mathbb{R}^{3\times3}$	Rotation matrix from frame Σ_a to frame Σ_b
$\alpha_1, \alpha_2, \alpha_3$	Euler angles representing $\boldsymbol{R}_c^v = \boldsymbol{R}_z(\alpha_1)\boldsymbol{R}_y(\alpha_2)\boldsymbol{R}_z(\alpha_3)$
$\boldsymbol{t}_{ab}^a \in \mathbb{R}^3$	Origin of frame Σ_b with respect of the origin of frame Σ_a expressed in Σ_a
$\boldsymbol{A}_a^b \in \mathbb{R}^{4\times4}$	Homogeneous transformation from frame Σ_a to frame Σ_b
$\overline{\mathbf{p}}$	Homogeneous representation of vector $\mathbf{p}$
$\mathbf{p}^{\mathrm{o}} \in \mathbb{R}^3$	Landmark position expressed in the inertial frame
$\mathbf{p}^{\mathrm{c}} \in \mathbb{R}^3$	Landmark position expressed in camera frame
$[p_u \;\; p_v]^T$	Pixel in the image plane
$\boldsymbol{f}_c \in \mathbb{R}^2$	Camera focal length expressed in pixel
k_r	Camera radial distortion coefficient
P	Number of different poses used for calibration
$N = P(P-1)/2$	Number of possible combinations of couples of poses

2 Background

In the following, the problem to be solved, together with the main geometrical relationships and the parameters to be estimated will be presented in detail. In particular, all relevant quantities and symbols are listed in Table 1 (see also Fig. 2. In Fig. 1, a picture of the mobile robot Khepera III holding a video camera used in the experiments is shown. The kinematic structure and the main quantities of the above robot is

Fig. 1 Picture of a mobile robot holding a video-camera

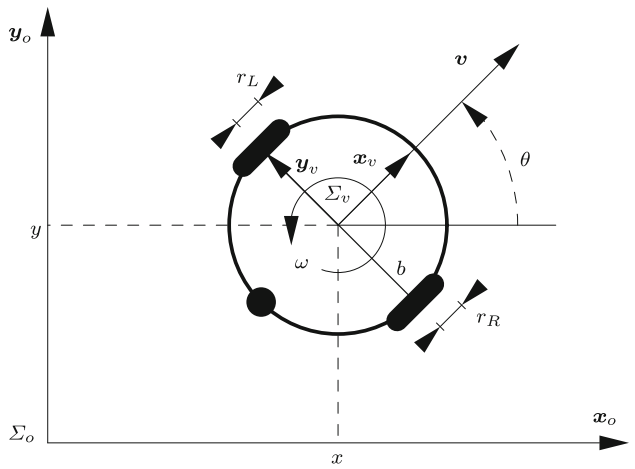

Fig. 2 Top-view sketch of a differential-drive mobile robot with relevant variables (without camera-fixed frame)

shown in Fig. 2; while in Fig. 3 a sketch of the camera-vehicle geometry is presented.

2.1 Unicycle kinematics

Consider the differential-drive mobile robot depicted in Fig. 2. Let x and y be the coordinates of the origin of the vehicle frame Σ_v, expressed in the inertial frame Σ_o, θ be the heading angle between the x-axes of Σ_v and Σ_o, v and ω be the vehicle linear and angular velocities, respectively. The vehicle kinematics is given by

$$\begin{cases} \dot{x} = v\cos(\theta) \\ \dot{y} = v\sin(\theta) \\ \dot{\theta} = \omega. \end{cases} \tag{1}$$

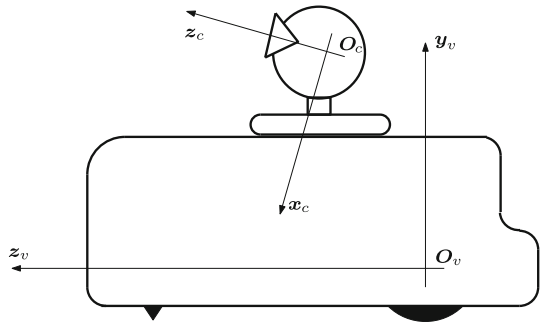

Fig. 3 Side-view sketch of a differential-drive mobile robot holding a video-camera

It can be recognized that the body-fixed components, v and ω, of the robot velocity are related to the left and right angular wheels velocities, ω_L and ω_R, respectively, by the following relation:

$$\begin{cases} v = \frac{r_R}{2}\,\omega_R + \frac{r_L}{2}\,\omega_L \\ \omega = \frac{r_R}{b}\,\omega_R - \frac{r_L}{b}\,\omega_L, \end{cases} \tag{2}$$

in which r_R and r_L are the radii of the right and left wheels, respectively, and b is the length of the wheels axis.

2.2 Frames relationships in different vehicle's poses

It is assumed that the considered vehicle is equipped with an on-board video-camera; let Σ_c be the corresponding attached frame.

Let $\boldsymbol{R}_o^c \in \mathbb{R}^{3\times 3}$ be the rotation matrix from the inertial frame to the camera frame, $\mathbf{p^c} \in \mathbb{R}^3$ be the coordinates of a generic point in the space (e.g., a landmark) expressed in the camera frame, and $\boldsymbol{t}_{co}^c \in \mathbb{R}^3$ be the vector of the origin of the inertial frame with respect to the origin of the camera frame, expressed in the camera frame. It is possible to define the following homogeneous transformation matrix:

$$\boldsymbol{A}_o^c = \begin{bmatrix} \boldsymbol{R}_o^c & \boldsymbol{t}_{co}^c \\ \mathbf{0}^{\mathrm{T}} & 1 \end{bmatrix} \tag{3}$$

where $\mathbf{0}$ is the (3×1) null vector and the homogeneous vector is given by

$$\overline{\mathbf{p}}^c = \begin{bmatrix} \mathbf{p^c}^{\mathrm{T}} & 1 \end{bmatrix}^{\mathrm{T}}. \tag{4}$$

The following holds

$$\overline{\mathbf{p}}^c = \boldsymbol{A}_o^c\,\overline{\mathbf{p}}^o. \tag{5}$$

Matrices $\boldsymbol{A}_o^v$ and $\boldsymbol{A}_c^v$ can be defined in the same way.

Let us now consider different vehicle *poses*, where the term pose denotes a configuration at which the vehicle is still; a numbered subscript univocally indicates a specific pose. Let us now also introduce the homogeneous transformations

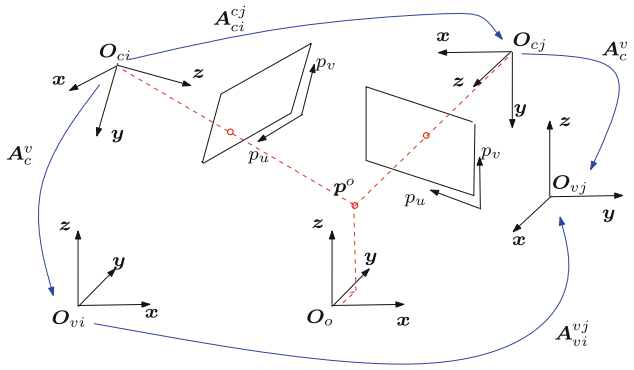

Fig. 4 Sketch with the frames definition. In particular, they are represented the vehicle frame, the camera frame, and the projection of an inertial landmark on the image plane in two different poses of the vehicle

$\boldsymbol{A}_{ci}^{cj}$ and $\boldsymbol{A}_{vi}^{vj}$ (see Fig. 4), where the subscripts i and j denote two different poses.

It can be shown that [18,16]

$$\boldsymbol{A}_c^v \, \boldsymbol{A}_{ci}^{cj} = \boldsymbol{A}_{vi}^{vj} \, \boldsymbol{A}_c^v, \tag{6}$$

where the subscripts i and j have been omitted in $\boldsymbol{A}_c^v$, since this matrix is constant. Equation (6) can be decomposed into the rotational and translational parts as follows:

$$\boldsymbol{R}_c^v \, \boldsymbol{R}_{ci}^{cj} = \boldsymbol{R}_{vi}^{vj} \, \boldsymbol{R}_c^v \tag{7}$$

$$\boldsymbol{R}_c^v \, \boldsymbol{t}_{cjci}^{cj} - \boldsymbol{t}_{vjvi}^{vj} = \boldsymbol{R}_{vi}^{vj} \, \boldsymbol{t}_{vc}^v - \boldsymbol{t}_{vc}^v. \tag{8}$$

Since $\boldsymbol{A}_o^c$ can be obtained for all the poses, e.g., via a vision calibration procedure, $\boldsymbol{A}_{ci}^{cj}$ can be computed as follows:

$$\boldsymbol{A}_{ci}^{cj} = \boldsymbol{A}_o^{cj} \, \boldsymbol{A}_{ci}^o. \tag{9}$$

As noticed in, e.g., [5], the motion of the vehicle, which is constrained to be planar, does not allow to identify all the unknowns of Eq. (6) (or, equivalently, in Eqs. (7),(8)). However, the following derivation, inspired by the work in [5], shows how to project (7) to determine the relevant quantities on the basis of the available motion variables. In detail, the vehicle rotates only around the z-axis of the inertial frame, i.e.,

$$\boldsymbol{R}_{vi}^{vj} = \boldsymbol{R}_z \, (\theta_{ij}) \tag{10}$$

where $\boldsymbol{R}_z(\theta_{ij})$ is the matrix expressing an elementary rotation around the z-axis of a reference frame [17]. Hence, Eq. (7) becomes

$$\boldsymbol{R}_v^c \boldsymbol{R}_z(\theta_{ij}) \boldsymbol{R}_c^v = \boldsymbol{R}_{ci}^{cj}. \tag{11}$$

It is possible to represent the rotation matrix $\boldsymbol{R}_c^v$ in terms of ZYZ Euler angles elementary rotations, i.e., as the composition of elementary rotations around coordinate axes of the inertial frame

$$\boldsymbol{R}_c^v = \boldsymbol{R}_z(\alpha_1) \boldsymbol{R}_y(\alpha_2) \boldsymbol{R}_z(\alpha_3). \tag{12}$$

Hence, the following holds

$$\boldsymbol{R}_z(-\alpha_3) \boldsymbol{R}_y(-\alpha_2) \boldsymbol{R}_z(-\alpha_1) \boldsymbol{R}_z(\theta_{ij}) \boldsymbol{R}_z(\alpha_1) \boldsymbol{R}_y(\alpha_2) \boldsymbol{R}_z(\alpha_3) = \boldsymbol{R}_{ci}^{cj}. \tag{13}$$

Since successive rotations around the same axis are commutative, the above equation can be simplified as follows and will be used in the following:

$$\boldsymbol{R}_z(-\alpha_3) \boldsymbol{R}_y(-\alpha_2) \boldsymbol{R}_z(\theta_{ij}) \boldsymbol{R}_y(\alpha_2) \boldsymbol{R}_z(\alpha_3) = \boldsymbol{R}_{ci}^{cj}. \tag{14}$$

2.3 Pinhole model

The camera model corresponds to a standard pin-hole projection with radial distortion truncated at the first term (see, e.g., [9]). Let

$$\boldsymbol{f}_c = \begin{bmatrix} f_{c,u} & f_{c,v} \end{bmatrix}^{\mathrm{T}} \in \mathbb{R}^2$$

be the effective focal lengths,

$$\boldsymbol{c}_c = \begin{bmatrix} c_{c,u} & c_{c,v} \end{bmatrix}^{\mathrm{T}} \in \mathbb{R}^2$$

be the principal point, both expressed in pixels, and k_r be the radial distortion coefficient. The vector

$$\mathbf{p^c} = \begin{bmatrix} x^c & y^c & z^c \end{bmatrix}^{\mathrm{T}} \in \mathbb{R}^{\mathbf{3}}$$

represents the coordinates of a point expressed in the camera reference frame (in meter). The pin-hole projection is defined by the following equations:

$$p_u = f_{c,u} \left\{ 1 + k_r \left[\left(\frac{x^c}{z^c} \right)^2 + \left(\frac{y^c}{z^c} \right)^2 \right] \right\} \frac{x^c}{z^c} + c_{c,u}$$

$$p_v = f_{c,v} \left\{ 1 + k_r \left[\left(\frac{x^c}{z^c} \right)^2 + \left(\frac{y^c}{z^c} \right)^2 \right] \right\} \frac{y^c}{z^c} + c_{c,v},$$

where p_u and p_v are the coordinates expressed in pixels. Of course, the given point can be expressed in a different reference frame, e.g., the inertial frame, by the known relation (in homogeneous coordinates)

$$\overline{\mathbf{p}}^o = \boldsymbol{A}_c^o \overline{\mathbf{p}}^c.$$

3 Problem formulation and proposed solution

It is assumed that a set of landmarks, of known inertial positions, are provided (one example can be found in Fig. 7). Let us further assume that the following sensing devices are available:

- incremental or absolute encoders mounted at the shafts of vehicle's wheels,
- a video-camera mounted on the vehicle body.

Additional external sensing devices are not needed.

It is required to calibrate, simultaneously

- the intrinsic camera parameters (three parameters: $f_{c,u}$, $f_{c,v}$ and k_r);
- the vehicle's odometry (three parameters: r_R, r_L and b);
- the camera-vehicle homogeneous transformation (the six independent parameters in $\boldsymbol{A}_c^v$: $\alpha_1, \alpha_2, \alpha_3$ in (12), and t_{vc}^v).

The solution consists in moving the robot in P configurations (poses); in each pose a snapshot of the landmarks is acquired by the camera with the robot still and, during the motion, the encoders data are recorded.

The following steps, detailed in next subsections, are then implemented:

1. Individual camera calibration for all the poses: camera extrinsic parameters $\boldsymbol{A}_o^{cj}$ for each pose and camera intrinsic parameters j, $f_{c,u}$, $f_{c,v}$, k_r (see Sect. 3.1);
2. Estimation of two intermediate odometric parameters: α_R and α_L and then used in Step 4 (see Sect. 3.2);
3. Estimation of two of the angles of $\boldsymbol{R}_c^v$: α_2 and α_3 in Eq. (12) (see Sect. 3.3);
4. Estimation of the remaining parameters: α_1 in Eq. (12), $\boldsymbol{t}_{vc}^v$ and r_L (see Sect. 3.4).

3.1 Step 1: camera calibration

For each of the P poses an independent camera calibration procedure is set-up. The intrinsic parameters $f_{c,u}$, $f_{c,v}$, and k_r, as well as the homogeneous transformation matrices $\boldsymbol{A}_o^{cj}$ for $j = \{1, \ldots, P\}$, are then estimated. Vision calibration is an assessed topic in the literature and the several effective algorithm can be adopted; in this paper the calibration is performed with an algorithm based on the minimization of a proper objective function by resorting to the Gauss–Newton method, see, e.g., [13].

It is worth noticing that, once matrices $\boldsymbol{A}_o^{cj}$ are estimated, all the matrices $\boldsymbol{A}_{ci}^{cj}$ (with $i, j = \{1, \ldots, P\}$), expressing the relative configuration between poses i and j can be computed via (9).

3.2 Step 2: estimation of intermediate odometric parameters

In order to obtain a linear-in-the-parameters relationship describing the vehicle odometry, the following parameters are defined [1]:

$$\alpha_R = \frac{r_R}{b}, \tag{15}$$

$$\alpha_L = -\frac{r_L}{b}, \tag{16}$$

which satisfy the relationship

$$r_R = -\frac{\alpha_R}{\alpha_L} r_L.$$

Equations (15)–(16) allow to rewrite the angular velocity in Eq. (2) as follows:

$$\omega = \alpha_R \omega_R + \alpha_L \omega_L. \tag{17}$$

By integrating (17) between the time instants $t_1 = 0$ and $t_2 = t$, and assuming, without loss of generality, $\theta(0) = 0$, one obtains

$$\theta(t) = \alpha_R \int_0^t \omega_R(\tau) \mathrm{d}\tau + \alpha_L \int_0^t \omega_L(\tau) \mathrm{d}\tau, \tag{18}$$

which can be rewritten as

$$\theta(t) = \alpha_R \theta_R(t) + \alpha_L \theta_L(t)\,, \tag{19}$$

where $\theta_R(t), \theta_L(t)$ represent the encoder positions of the right and left wheel, respectively. The linear relationship between the coefficients α_R, α_L and θ is obvious; in fact, at the generic time instant $t = t_k$ it is possible to write

$$\theta_k = \boldsymbol{\Phi}_{\theta_k} \begin{bmatrix} \alpha_R \\ \alpha_L \end{bmatrix}, \tag{20}$$

with

$$\theta_k = \theta(t_k) \quad \boldsymbol{\Phi}_{\theta_k} = \begin{bmatrix} \theta_R(t_k) & \theta_L(t_k) \end{bmatrix}. \tag{21}$$

The angles θ_k can be measured, by taking N different couple of poses (i, j), from the relative camera orientation matrix (i.e., $\boldsymbol{R}_{ci}^{cj}$) by using Eq. (24) and considering that the camera and vehicle frames are subject to the same orientation displacements around the vertical axis (i.e., the z-axis) of the inertial frame. By collecting $N \geq 2$ samples θ_k, Eq. (20) gives

$$\begin{bmatrix} \theta_1 \\ \vdots \\ \theta_N \end{bmatrix} = \begin{bmatrix} \boldsymbol{\Phi}_{\theta_1} \\ \vdots \\ \boldsymbol{\Phi}_{\theta_N} \end{bmatrix} \begin{bmatrix} \alpha_R \\ \alpha_L \end{bmatrix} = \overline{\boldsymbol{\Phi}}_\theta \begin{bmatrix} \alpha_R \\ \alpha_L \end{bmatrix}. \tag{22}$$

The reconstruction error over the angle data collected in the N samples is then minimized in a least-squares sense by estimating the unknown parameters α_R and α_L as follows:

$$\begin{bmatrix} \hat{\alpha}_R \\ \hat{\alpha}_L \end{bmatrix} = \left(\overline{\boldsymbol{\Phi}}_\theta^{\mathrm{T}} \overline{\boldsymbol{\Phi}}_\theta \right)^{-1} \overline{\boldsymbol{\Phi}}_\theta^{\mathrm{T}} \begin{bmatrix} \theta_1 \\ \vdots \\ \theta_N \end{bmatrix}. \tag{23}$$

It must be noticed that $P \geq 3$ poses are required to perform this step, so as to obtain $N \geq 2$ samples for θ. In addition, it can be easily verified that, if the measured rotations angles are equal or multiple of each other, the regressor is numerically badly scaled. From a practical point of view, this is simply avoided by selecting asymmetric poses around the calibration tool.

3.3 Step 3: estimation of α_2 and α_3

Angles α_2 and α_3 can be computed from matrix $\boldsymbol{R}_{ci}^{cj}$, taken in different couple of poses $(i,\ j)$, as described in the following.

The left-hand side of (14) corresponds to the usual definition of axis-angle representation of the orientation [17] (with the proper angles' sign). Since $\boldsymbol{R}_{ci}^{cj}$ can be computed via (9), θ_{ij}, α_2 and α_3, can be computed. In detail [17]

$$\theta_{ij} = \cos^{-1}\left(\frac{R_{11}+R_{22}+R_{33}-1}{2}\right), \tag{24}$$

where R_{pq} denotes the generic element of $\boldsymbol{R}_{ci}^{cj}$. The rotation axis

$$\boldsymbol{r} = \begin{bmatrix} r_x \\ r_y \\ r_z \end{bmatrix} = \frac{1}{2\sin\theta_{ij}} \begin{bmatrix} R_{32}-R_{23} \\ R_{13}-R_{31} \\ R_{21}-R_{12} \end{bmatrix} \tag{25}$$

allows to compute α_2 and α_3 as follows:

$$\alpha_2 = \text{atan2}\left(\sqrt{r_x^2+r_y^2}, r_z\right), \tag{26}$$

$$\alpha_3 = \text{atan2}(r_y, -r_x). \tag{27}$$

Equation (14) shows that condition $\theta_{ij} \neq 0$ is required to avoid a trivial equation satisfied by an arbitrary axis–angle couple. The physical interpretation is obvious: a nontrivial vehicle rotation is needed to estimate the relevant variables of the left-hand side of (14).

It must be noticed that at least $P = 2$ poses are required to estimate $\boldsymbol{r}$, α_2 and α_3. Of course, a larger number of poses may be exploited to improve the estimation results.

3.4 Step 4: estimation of α_1, $\mathbf{t}_{vc}^{v}$ and r_L

In order to estimate the angle α_1 in $\boldsymbol{R}_c^v$, the planar components of $\boldsymbol{t}_{vc}^v$ and r_L, Eq. (8) have to be used. Unidentifiability of the vertical component of $\boldsymbol{t}_{vc}^v$ (i.e., along the z-axis of the inertial frame) can be understood by direct observation of the fact that the third equation (8) is identically satisfied for any set of data physically achievable with the given robot planar mobility [5].

Let us now analyze and rewrite in a different form Eq. (8) in order to estimate the remaining unknown parameters. Vector $\boldsymbol{t}_{cjci}^{cj}$ is known from the vision calibration (step 1), by resorting to the relationship (9). The rotation matrix $\boldsymbol{R}_c^v$, expressed in terms of three elementary rotations $\boldsymbol{R}_c^v = \boldsymbol{R}_z(\alpha_1)\boldsymbol{R}_y(\alpha_2)\boldsymbol{R}_z(\alpha_3)$, is a function of the unknown α_1, since α_2 and α_3 are already available from step 3. The vector $\boldsymbol{t}_{vjvi}^{vj}$ represents the vehicle displacement between two generic poses, expressed with respect to the final frame Σ_{vj}; integration of Eq. (1) gives the displacement expressed in the initial pose, $\boldsymbol{t}_{vivj}^{vi}$. As shown in [1], the following discrete-time equations for the position displacement can be devised from (1)

$$\begin{bmatrix} x_{k+1}-x_k \\ y_{k+1}-y_k \end{bmatrix} = \frac{T}{2}\begin{bmatrix} \left(-\dfrac{\alpha_R}{\alpha_L}\,\omega_{R,k}+\omega_{L,k}\right)\cos\left(\theta_k+\dfrac{T\omega_k}{2}\right) \\ \left(-\dfrac{\alpha_R}{\alpha_L}\,\omega_{R,k}+\omega_{L,k}\right)\sin\left(\theta_k+\dfrac{T\omega_k}{2}\right) \end{bmatrix} r_L,$$

where the subscript k denotes the kth time sample and T is the sampling period. Clearly, the above equation defines a linear mapping between r_L and the position displacement. In particular, the relationship between the kinematic quantities at a generic time step (corresponding to pose i), $k = 0$, and final time step (corresponding to pose j), $k = K$, is

$$\begin{aligned} \boldsymbol{t}_{vivj}^{vi} &= \begin{bmatrix} x_K - x_0 \\ y_K - y_0 \end{bmatrix} \\ &= \frac{T}{2}\begin{bmatrix} -\dfrac{\alpha_R}{\alpha_L}\displaystyle\sum_{k=0}^{K-1}\omega_{R,k}\,c_k + \sum_{k=0}^{K-1}\omega_{L,k}\,c_k \\ -\dfrac{\alpha_R}{\alpha_L}\displaystyle\sum_{k=0}^{K-1}\omega_{R,k}\,s_k + \sum_{k=0}^{K-1}\omega_{L,k}\,s_k \end{bmatrix} r_L, \end{aligned} \tag{28}$$

where $c_k = \cos(\theta_k + T\omega_k/2)$ and $s_k = \sin(\theta_k + T\omega_k/2)$. It is worth noticing that θ_k and ω_k in Eq. (28) can be computed from Eq. (17) and Eq. (18), respectively, since α_R and α_L have already been identified in Step 2 (see Sect. 3.2).

By using Eq. (28), Eq. (8) can be then rewritten compactly as

$$\boldsymbol{t}_{vivj}^{vi} = \begin{bmatrix} \beta_1 \\ \beta_2 \\ 0 \end{bmatrix} r_L = \boldsymbol{\beta}_{ij}\, r_L\,, \tag{29}$$

with an implicit definition of the two known coefficients β_1 and β_2.

Equation (8) can be rewritten as follows:

$$\boldsymbol{R}_c^v\,\boldsymbol{t}_{cjci}^{cj} + \boldsymbol{R}_{vi}^{vj}\,\boldsymbol{\beta}_{ij}\,r_L - \left(\boldsymbol{R}_{vi}^{vj} - \boldsymbol{I}\right)\boldsymbol{t}_{vc}^v = \boldsymbol{0}. \tag{30}$$

The first two rows of the above equation system are those to be considered for the estimation of the unknown parameters. Indeed, the left-hand side of the above equation contains $\boldsymbol{R}_c^v$, that is nonlinear with respect to α_1. However, the term $\boldsymbol{R}_c^v\,\boldsymbol{t}_{cjci}^{cj}$ can be rewritten in a form linear in $s_{\alpha_1} = \sin(\alpha_1)$ and $c_{\alpha_1} = \cos(\alpha_1)$. Hence, Eq. (30) can be rewritten in a form linear in the new remaining unknown parameters: $\left[r_L\ t_{vc,x}^v\ t_{vc,y}^v\ c_{\alpha_1}\ s_{\alpha_1}\right]$.

For the sake of notation compactness, let us define the index $l \in \{1,\ldots,N\}$ representing a couple of poses (indexed, in turn, by $i \in \{1,\ldots,P\}$ and $j \in \{1,\ldots,P\}$). Then, the

first two components of Eq. (30) become

$$\boldsymbol{\Phi}_l\,\boldsymbol{\zeta} = \left[\, \boldsymbol{R}_{\theta,l}\;\boldsymbol{\beta}_l\;\boldsymbol{T}_{\theta,l}\;\boldsymbol{T}_{\alpha,l}\,\right] \begin{bmatrix} r_L \\ t^v_{vc,x} \\ t^v_{vc,y} \\ c_{\alpha_1} \\ s_{\alpha_1} \end{bmatrix} = \mathbf{0}, \tag{31}$$

with

$$\boldsymbol{T}_{\theta,l} = \boldsymbol{I} - \boldsymbol{R}_{\theta,l}$$

$$\boldsymbol{R}_{\theta,l} = \begin{bmatrix} c_{\theta_l} & -s_{\theta_l} \\ s_{\theta_l} & c_{\theta_l} \end{bmatrix}$$

$$s_{\theta_l} = \sin\left(\theta_{ij}\right)\,, \quad c_{\theta_l} = \cos\left(\theta_{ij}\right)$$

$$\boldsymbol{T}_{\alpha,l} = \begin{bmatrix} a_l & -b_l \\ b_l & a_l \end{bmatrix}$$

$$a_l = c_{\alpha_2}c_{\alpha_3}t^{cj}_{cjci,x} - c_{\alpha_2}s_{\alpha_3}t^{cj}_{cjci,y} + s_{\alpha_2}t^{cj}_{cjci,z}$$

$$b_l = s_{\alpha_3}t^{cj}_{cjci,x} + c_{\alpha_3}t^{cj}_{cjci,y}\,,$$

where $\boldsymbol{R}^{vj}_{vi}$ has been expressed, as in (10), in terms of an elementary rotation around the z-axis of the inertial frame.

Equation (31) can be written for each of the N available couple of poses, giving

$$\begin{bmatrix} \boldsymbol{\Phi}_1 \\ \vdots \\ \boldsymbol{\Phi}_N \end{bmatrix} \boldsymbol{\zeta} = \boldsymbol{\Phi}\boldsymbol{\zeta} = \mathbf{0}, \tag{32}$$

where $\boldsymbol{\Phi} \in \mathbb{R}^{2N\times 5}$. Moreover, $\boldsymbol{\zeta}$ is subject to the constraint (imposed by the relation $c^2_{\alpha_1} + s^2_{\alpha_1} = 1$):

$$\zeta_4^2 + \zeta_5^2 = 1.$$

In the Appendix, it is shown that, with a proper choice of the robot's poses, the regressor matrix is such that $\mathrm{rank}(\boldsymbol{\Phi}) = 4$. Thus, $\boldsymbol{\Phi}$ has a 1-dimensional null space which can be determined by computing the orthonormal (5×5) matrix, $\boldsymbol{V}$, of the Singular Value Decomposition (SVD) [8]:

$$\boldsymbol{\Phi} = \boldsymbol{U}\boldsymbol{\Sigma}\boldsymbol{V}^T, \tag{33}$$

where the matrix $\boldsymbol{\Sigma} \in \mathbb{R}^{2N\times 5}$ contains along the main diagonal the five non-negative singular values listed in decreasing order with respect to their magnitude. It is now clear that the fifth column of $\boldsymbol{V}$, $\boldsymbol{v}_5$, spans the null space of $\boldsymbol{\Phi}$. Hence, the solution to (32) has the form

$$\boldsymbol{\zeta}^* = \kappa\,\boldsymbol{v}_5,$$

with κ a constant value to be determined. Among the infinite solutions the one of interest is the sole value that satisfies the constraint $\zeta_4^2 + \zeta_5^2 = 1$, which can be easily computed by choosing

$$\kappa = \frac{1}{\sqrt{v^2_{5,4} + v^2_{5,5}}}. \tag{34}$$

Once r_L is known, it is trivial to obtain r_R and b from (15)–(16):

$$\hat{r}_R = -\frac{\hat{\alpha}_R}{\hat{\alpha}_L}\hat{r}_L \tag{35}$$

$$\hat{b} = \frac{\hat{r}_R}{\hat{\alpha}_R} \quad \text{or} \quad \hat{b} = -\frac{\hat{r}_L}{\hat{\alpha}_L}. \tag{36}$$

4 Simulations

Before testing the approach on a real setup, the proposed solution has been tested in simulation. It is easy to imagine that, as the above procedure does not imply any approximation, it is able, in ideal conditions, to exactly identify the required parameters up to the machine precision. Extensive numerical simulations have been carried out to verify the validity of the proposed approach in the presence of unavoidable practical approximations as, for example, the camera and encoder quantization and the sampling time, etc. Then, the main algorithm parameters have been varied in order to test numerically the robustness with respect to possible changes in the problem conditions.

In the simulations the sample time has been set to a reasonable value of $T = 0.02\,\mathrm{s}$, corresponding to cheap microcontrollers running soft real-time code. It is worth noticing that low sampling frequencies and high vehicle velocities can be a significant source of odometric errors. When it is not possible to increase the sampling frequency due to hardware limitations, it is obviously convenient to move the vehicle among the poses at relatively low velocity.

Pixel quantization for a 640×480 video-camera as well as a 0.1302° encoder quantization has been further added in order to reproduce the same experimental conditions. In such conditions, only $P = 5$ poses are sufficient to achieve a relative error of 0.1% on the odometry parameters and 1% on the vehicle-camera roto-translation matrix over a 0.25 average pixel error in the calibration procedure.

Moreover, looking at the numerical value of matrix $\boldsymbol{\Phi}$ in Eq. (32), the ratio σ_5/σ_4 of the last and the next-to-last singular values is typically 10^{-3}, while $\sigma_4/\sigma_3 = 0.8$, according to the property of $\boldsymbol{\Phi}$ to be a 4-rank matrix. Indeed, in ideal conditions, σ_5 should be zero, but noise, quantization, and numerical integration (used to derive Eq. (29)) do not yield such a condition rigorously. This situation mainly arises in experiment (where also slippage, misaligned wheels, and other effects are present) and some words need to be spent. Because of noise, the matrix $\boldsymbol{\Phi}$ is not rigorously a 4-rank matrix. Then, considering the fifth column of matrix $\boldsymbol{V}$ in Eq. (33) as a basis of the null space of matrix $\boldsymbol{\Phi}$ means to approximate $\boldsymbol{\Phi}$ with a new matrix $\widetilde{\boldsymbol{\Phi}} = \boldsymbol{U}\widetilde{\boldsymbol{\Sigma}}\boldsymbol{V}^T$, where $\boldsymbol{U}$ and $\boldsymbol{V}$ are the same matrices obtained by the Singular Value Decomposition of matrix $\boldsymbol{\Phi}$, and the matrix $\widetilde{\boldsymbol{\Sigma}}$ differs from $\boldsymbol{\Sigma}$

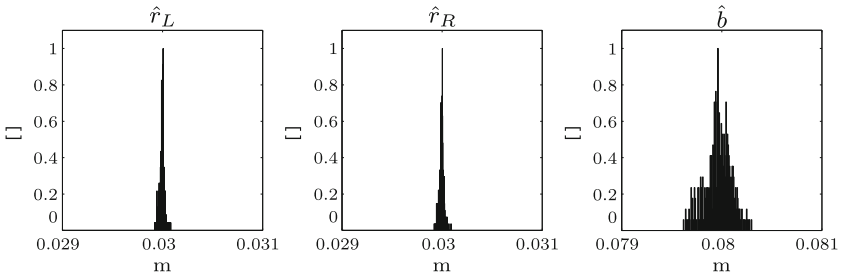

Fig. 5 Normalized histogram of the distribution of the left and right radii estimation

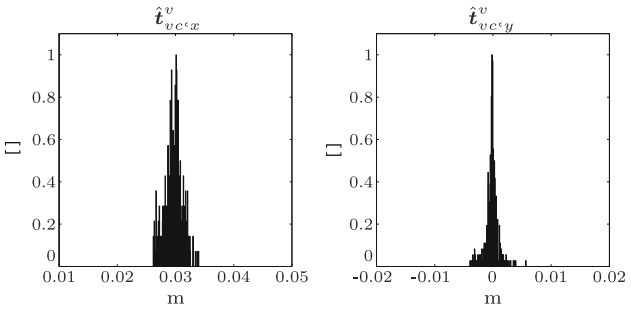

Fig. 6 Normalized histogram of the distribution of x and y estimated components of $\boldsymbol{t}^v_{vc}$

only in the 5th element of its main diagonal that is set to zero. This means that $\widetilde{\boldsymbol{\Phi}}$ is a 4-rank matrix and is different from the original one. However, the Eckart–Young theorem [10] states that the so obtained matrix $\widetilde{\boldsymbol{\Phi}}$ minimizes the Frobenius norm of the difference between $\boldsymbol{\Phi} - \widetilde{\boldsymbol{\Phi}}$ under the constraint that $\text{rank}(\widetilde{\boldsymbol{\Phi}}) = 4$.

In the following, several simulations have been performed considering several trajectories with $P = 15$ (in order to improve precision). The results of the different simulations have been collected in order to draw the distribution of the estimated parameters. The real odometry parameters used in the simulation are $r_L = r_R = 0.03\,\text{m}$ and $b = 0.08\,\text{m}$, while the camera-vehicle rotation matrix is $\boldsymbol{R}^v_c = \boldsymbol{R}_z(\alpha_1)\boldsymbol{R}_y(\alpha_2)\boldsymbol{R}_z(\alpha_3) = \boldsymbol{R}_z(0)\boldsymbol{R}_y(1.396)\boldsymbol{R}_z(0)$ where the angles are expressed in radians. Finally, it has been assumed $\boldsymbol{t}^v_c = \begin{bmatrix}0.03 & 0 & 0\end{bmatrix}\text{m}$. In Fig. 5, they are shown the distributions of the identified odometry parameters (indicated by the $\hat{(\cdot)}$ symbol). These figures are interesting as they show that the estimated parameters distribute along the bell-shaped curves around the respective exact value. In Fig. 6, the same histograms are shown for the first two components of the vector $\boldsymbol{t}^v_c$ and, also in this case, the estimated values distributed around the exact ones. The same happens for the three euler angles of rotation matrix $\boldsymbol{R}^v_{vc}$; graphs have been omitted for brevity.

Moreover and as expected, other performed simulations showed that the precision of the estimated parameters (and consequently the standard deviation of the estimated parameters distributions) strongly relies on the encoder's resolution and the sample time. However, errors caused by these quantities can be partially contained by slowly moving the robot.

On the contrary, the camera resolution and the camera calibration procedure heavily affect the obtained results, as all the steps 2–4 rely on the estimation of $\boldsymbol{R}^{ci}_{cj}$ and the extracted rotation angle θ around the vertical inertial axis. This means that the camera and the calibration tool need to be properly chosen in order to obtain the desired estimation precision. However, given a camera, better results can be obtained by designing the calibration tool with an high number of landmarks, and the robot's poses in order to maximize the distribution of the markers along the image plane.

5 Experiments

The experimental setup is composed of a Khepera III differential drive robot manufactured by K-TEAM Corporation. The robot is equipped with a Linux-embedded operating system, a standard Logitech QuickCam Web Camera (with maximum resolution of 640×480 pixels), a WIFI communication card, and two wheel encoders (with $0.1302°$ resolution). The adopted sampling time is $T = 0.02$ s.

Calibration is performed by using a landmarks tool, i.e., a box with a 0.25×0.25 m base and height equal to 0.2 m (Fig. 7).

On each of the four lateral faces of the calibration box, a CAD-designed grid of 135 markers has been attached in

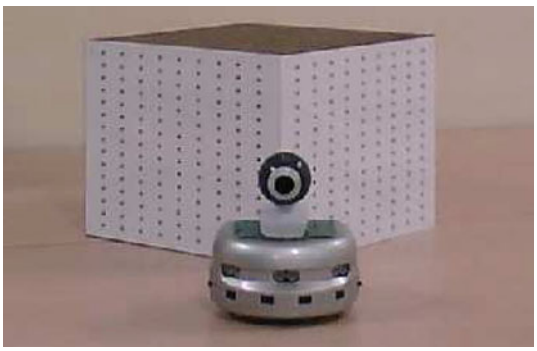

Fig. 7 The experimental setup

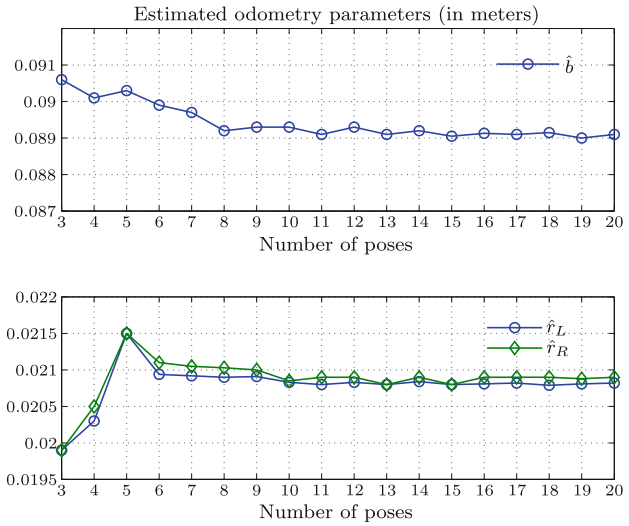

Fig. 8 Odometry parameter estimation over the poses number. *Top* estimated wheel axis length. *Bottom* estimated wheel radii

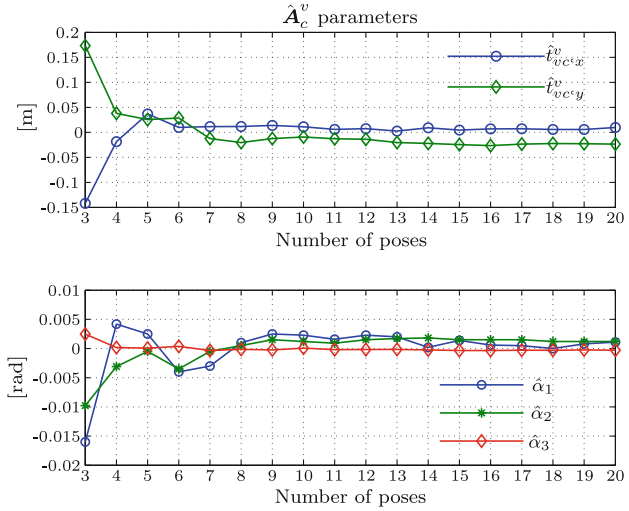

Fig. 9 $\hat{A}_c^v$ parameters over the poses number. *Top* translational components (translated toward zero by their mean value). *Bottom* ZYZ Euler angles (translated toward zero by their mean value) of the rotation matrix $\hat{R}_c^v$

such a way the markers' positions are known in the inertial reference frame, assumed to be coincident with the box reference frame. However, as described in Sects. 3.1–3.4, we are only interested in the matrices A_{cj}^{ci}; this means that the calibration of the camera can be performed by means of any of the methods and tools available in the literature.

In order to implement the proposed algorithm, the robot starts from a roughly known initial configuration towards P via points driven only by odometry (or by a wireless emulated joystick, in the case of completely unknown odometry parameters or long paths). At each via point the vehicle is stopped and a snapshot of the calibration box is taken, while the odometry data required by Eqs. (22)–(28) are saved. Notice that this procedure simplifies significatively the synchronization between the two different devices. According to the simulation results, in our experiments $P = 20$ via points path have been taken. The number of poses has to be intended here as chronological order, even if this is not required by the proposed approach. In addition, as it can be noticed from Sects. 3.1–3.4, the trajectory of the robot from one pose to the other does not matter as the change of the vehicle's orientation θ and the matrix A_{cj}^{ci} depend only on the initial and final poses. The same happens to the vector $t_{v1,v2}^{v1}$; however, longer and/or faster trajectories would lead to greater errors in the coefficients β_i in (29) due to the sample time and the wheels' slippage.

With regard to the camera calibration, the average pixel error is 0.5 pixels, corresponding to few millimeters over an average 0.6×0.6 m scene. Moreover, the mean values of the intrinsic camera parameters are $f_{c,u} = 1013$, $f_{c,v} = 1024$ and $k_r = 2 \times 10^{-7}$ with a very small variance.

Figure 8 shows the estimated odometry parameters $\hat{r}_L$, $\hat{r}_R$ and $\hat{b}$ over the number of poses.

It can be noticed that the estimated odometry parameters converge to steady-state values, i.e., $\hat{r}_L \approx 0.0208$ m, $\hat{r}_R \approx 0.0209$ m and $\hat{b} \approx 0.0891$ m. Moreover, the obtained values are very close to the nominal values given by the K-Team Corporation (i.e., 0.021 m for the wheels' radius and 0.09 m for the wheel base length) and to the values computed in [4].

As for the vehicle-camera roto-translation matrix $\hat{A}_c^v$, Fig. 9 shows the translation components $\hat{t}^v_{vc,x}$, $\hat{t}^v_{vc,y}$ and the ZYZ Euler angles $\hat{\alpha}_1, \hat{\alpha}_2, \hat{\alpha}_3$ corresponding to the rotation matrix $\hat{R}_c^v$ over the poses number; the vectors have been eventually translated of 90° towards zero to reduce the y-axis range and improve the view of the parameters' trend.

From Fig. 9, it can be noticed as, also in this case, the roto-translation matrix $\hat{A}_c^v$ reaches a steady-state value:

$$\hat{A}_c^v = \begin{bmatrix} -0.0338 & 0.0531 & 0.9980 & 0.0311 \\ 0.0020 & 0.9986 & -0.0531 & -0.0011 \\ -0.9994 & 0.0002 & -0.0339 & 0.1123 \\ 0 & 0 & 0 & 1 \end{bmatrix}, \quad (37)$$

where the translational components are expressed in meters and the $\hat{t}^v_{vc,z}$ component has been found constraining the origin of the vehicle reference frame on the inertial $x - y$ plane.

Finally, the analysis of the singular values of the matrix $\boldsymbol{\Phi}$ shows as, in our experiments, the ratio σ_5/σ_4 is close to 5×10^{-2}, while $\sigma_4/\sigma_3 \approx 0.7$, according to the rank property of the matrix $\boldsymbol{\Phi}$. It is worth remarking that σ_5 is expected to be null in ideal conditions; of course, noise, quantization, and numerical errors allow to satisfy this condition only with a certain degree of accuracy.

6 Conclusions

In this paper a method for calibrating both robot odometric parameters and on-board sensing devices has been presented. In particular, it allows to simultaneously identify the robot odometry and camera parameters, together with the camera pose with respect to the vehicle. Knowledge of the nominal values of the parameters is not required. The method requires to adopt a set of landmarks, whose positions in a inertial reference frame is known and the robot to move randomly acquiring images of the landmarks. The approach has been proven to be effective also in the case of very inexpensive hardware, such as a Khepera III robot and a Logitech web camera. Future work is aimed at investigating the sensitivity of the proposed solution to the errors sources and at choosing the robot poses in such a way to better excite all the unknowns. Moreover, also the effects of wheel misalignment and other mechanical errors will be investigated.

Appendix: Rank property of matrix $\boldsymbol{\Phi}$

The matrix $\boldsymbol{\Phi}$ in Eq. (32) can be written for each of the N available combination of poses, giving

$$\boldsymbol{\Phi} = \begin{bmatrix} \boldsymbol{R}_{\theta,1}\boldsymbol{\beta}_1 & \boldsymbol{T}_{\theta,1} & \boldsymbol{T}_{\alpha,1} \\ \dots & \dots & \dots \\ \boldsymbol{R}_{\theta,N}\boldsymbol{\beta}_N & \boldsymbol{T}_{\theta,N} & \boldsymbol{T}_{\alpha,N} \end{bmatrix}.$$

It can be noticed that Eq. (32) implies that $\boldsymbol{\Phi}$ cannot be a full rank matrix; otherwise, the only solution to (32) would be the trivial one (i.e., $\boldsymbol{\zeta} = \boldsymbol{0}$), which is not possible, given the physical meaning of the parameters in $\boldsymbol{\zeta}$. Hence, $\text{rank}(\boldsymbol{\Phi}) \leq 4$.

In order to find a sufficient condition ensuring $\text{rank}(\boldsymbol{\Phi}) = 4$, consider two couples of poses, denoted by subscripts l and m, respectively, and the following submatrix of $\boldsymbol{\Phi}$:

$$\boldsymbol{\Phi}^{(l,m)} = \begin{bmatrix} \boldsymbol{T}_{\theta,l} & \boldsymbol{T}_{\alpha,l} \\ \boldsymbol{T}_{\theta,m} & \boldsymbol{T}_{\alpha,m} \end{bmatrix}. \tag{38}$$

Then, $\text{rank}(\boldsymbol{\Phi}^{(l,m)}) = 4$ would imply that $\text{rank}(\boldsymbol{\Phi}) = 4$, since the addition of rows and columns cannot decrease the rank.

Since matrices $\boldsymbol{T}_{\theta,\star}$ and $\boldsymbol{T}_{\alpha,\star}$ ($\star = l, m$) are (2×2) matrices composed by 2 orthogonal columns (rows), it can be easily proven that

- they have rank 2 if and only if they are nonnull;
- products between such matrices commute, i.e., $\boldsymbol{T}_{\theta,\star}\boldsymbol{T}_{\alpha,\star} = \boldsymbol{T}_{\alpha,\star}\boldsymbol{T}_{\theta,\star}$.

A necessary condition for $\text{rank}(\boldsymbol{\Phi}^{(l,m)}) = 4$ is that at least one of two blocks of $\boldsymbol{\Phi}^{(l,m)}$ lying on the same column (row) must be non-null, and thus full-rank. Hence, it can be assumed, without loss of generality, that $\boldsymbol{T}_{\theta,l} \neq \boldsymbol{O}$ (i.e., $\theta, l \neq 0$), and thus $\text{rank}(\boldsymbol{T}_{\theta,l}) = 2$. In this case, the well-known equality

$$\text{rank}\left(\begin{bmatrix} \boldsymbol{T}_{\theta,l} & \boldsymbol{T}_{\alpha,l} \\ \boldsymbol{T}_{\theta,m} & \boldsymbol{T}_{\alpha,m} \end{bmatrix}\right) = \text{rank}\left(\boldsymbol{T}_{\theta,l}\right) + \text{rank}\left(\boldsymbol{T}_{\alpha,m} - \boldsymbol{T}_{\theta,m}\boldsymbol{T}_{\theta,l}^{-1}\boldsymbol{T}_{\alpha,l}\right)$$

holds. Being $\text{rank}(\boldsymbol{T}_{\theta,l}) = 2$, the following equality follows:

$$\text{rank}\left(\boldsymbol{\Phi}^{(l,m)}\right) = 4 \Leftrightarrow \text{rank}\left(\boldsymbol{T}_{\alpha,m} - \boldsymbol{T}_{\theta,m}\boldsymbol{T}_{\theta,l}^{-1}\boldsymbol{T}_{\alpha,l}\right) = 2.$$

Since, $\text{rank}(\boldsymbol{T}_{\theta,l}) = \text{rank}(\boldsymbol{T}_{\theta,l}^{-1}) = 2$, it follows

$$\begin{aligned} &\text{rank}\left(\boldsymbol{T}_{\alpha,m} - \boldsymbol{T}_{\theta,m}\boldsymbol{T}_{\theta,l}^{-1}\boldsymbol{T}_{\alpha,l}\right) \\ &\quad = \text{rank}\left(\boldsymbol{T}_{\theta,l}^{-1}\left(\boldsymbol{T}_{\theta,l}\boldsymbol{T}_{\alpha,m} - \boldsymbol{T}_{\theta,m}\boldsymbol{T}_{\alpha,l}\right)\right) \\ &\quad = \text{rank}\left(\boldsymbol{T}_{\theta,l}\boldsymbol{T}_{\alpha,m} - \boldsymbol{T}_{\theta,m}\boldsymbol{T}_{\alpha,l}\right) = 2 \end{aligned}$$

where the commutativity property has been exploited. Since the matrix $\boldsymbol{T}_{\theta,l}\boldsymbol{T}_{\alpha,m} - \boldsymbol{T}_{\theta,m}\boldsymbol{T}_{\alpha,l}$ has the same structure of $\boldsymbol{T}_{\theta,\star}$ and $\boldsymbol{T}_{\alpha,\star}$ ($\star = l, m$), i.e., it is composed of 2 orthogonal columns (rows), it is possible to notice that the need for its full rank has an immediate interpretation in the properties of the matrices $\boldsymbol{T}_{\alpha,\star}$ and $\boldsymbol{T}_{\theta,\star}$:

$$\text{rank}\left(\boldsymbol{T}_{\theta,l}\boldsymbol{T}_{\alpha,m} - \boldsymbol{T}_{\theta,m}\boldsymbol{T}_{\alpha,l}\right) = 2 \Leftrightarrow \boldsymbol{T}_{\theta,l}\boldsymbol{T}_{\alpha,m} \neq \boldsymbol{T}_{\theta,m}\boldsymbol{T}_{\alpha,l}.$$

In sum, a sufficient condition ensuring $\text{rank}(\boldsymbol{\Phi}) = 4$ is

$$\boldsymbol{T}_{\theta,l}\boldsymbol{T}_{\alpha,m} \neq \boldsymbol{T}_{\theta,m}\boldsymbol{T}_{\alpha,l}. \tag{39}$$

A condition that arises from (39) is that all the matrices need to be different from the Null one. The immediate consequence is that trivial set of poses where, for example, for *all* the poses the orientation is not changed or, again for *all* the poses, there is no vehicle translation, needs to be avoided.

A further thought on Eq. (39) allows to understand why, in practice, any set of data leads to a 4-rank matrix $\boldsymbol{\Phi}$. It is sufficient, in fact, to notice that, given the matrices $\boldsymbol{T}_{\alpha,l}$, $\boldsymbol{T}_{\alpha,m}$ and $\boldsymbol{T}_{\theta,l}$ it is always possible to compute a value for $\boldsymbol{T}_{\theta,m}$, function of one single rotation angle, that satisfies condition (39). Thus, a rank smaller than 4 has to be interpreted as a singularity in the set of data that leads to infinite solutions. This situations can be easily avoided by not choosing trivial poses as discussed in previous paragraph and by verification of condition (39).

References

1. Antonelli G, Chiaverini S (2007) Linear estimation of the physical odometric parameters for differential-drive mobile robots. Auton Robots 23(1):59–68
2. Antonelli G, Chiaverini S, Fusco G (2005) A systematic calibration method for odometry of mobile robots based on the least-squares technique: theory and experimental validation. IEEE Trans Robot 21(5):994–1004

3. Borenstein J, Feng L (1996) Measurement and correction of systematic odometry errors in mobile robots. IEEE Trans Robot Autom 12(6):869–880
4. Censi A, Marchionni L, Oriolo G (2008) Simultaneous maximum-likelihood calibration of robot and sensor parameters. In: Proceedings of the IEEE international conference on robotics and automation (ICRA), 19–23 May
5. Chang YL, and Aggarwal JK (1991) Calibrating a mobile camera's extrinsic parameters with respect toits platform. In: Proceedings of the 1991 IEEE international symposium on intelligent control, pp 443–448
6. Doh N, Choset H, Chung WK (2003) Accurate relative localization using odometry. In: Proceedings 2003 IEEE international conference on robotics and automation, Taipei, TW, pp 1606–1612
7. Doh NL, Choset H, Chung WK (2006) Relative localization using path odometry information. Autonomous Robots 21(2):143–154
8. Golub GH, Van Loan CF (1996) Matrix computations, 3rd edn. The Johns Hopkins University Press, Baltimore
9. Hutchinson S, Hager GD, Corke PI (1996) A tutorial on visual servo control. IEEE Trans Robot Autom 12(5):551–570
10. Johnson RM (1963) On a theorem stated by Eckart and Young. Psychometrika 28(3):259–263
11. Kelly A (2001) General solution for linearized systematic error propagation in vehicle odometry. In: Proceedings 2001 IEEE/RSJ international conference on intelligent robots and systems, Maui, HI, pp 1938–1945
12. Kelly A (2002) General solution for linearized stochastic error propagation in vehicle odometry. In: Preprints 15th IFAC World Congress, Barcelona, Spain, July
13. Madsen K, Nielsen HB, Tingleff O (2004) Methods for non-linear least squares problems. Technical University of Denmark, Lyngby, DK
14. Martinelli A (2002) The accuracy on the parameter estimation of an odometry system of a mobile robot. In: Proceedings 2002 IEEE international conference on robotics and automation, Washington, DC, pp 1378–1383
15. Martinelli A (2002) The odometry error of a mobile robot with a synchronous drive system. IEEE Trans Robot Autom 18(3):399–405
16. Park FC, Martin BJ (1994) Robot sensor calibration: solving AX=XB on the Euclidean group. IEEE Trans Robot Autom 10(5):717–721
17. Siciliano B, Sciavicco L, Villani L, Oriolo G (2008) Robotics: modelling, planning and control, 3rd edn. Springer, London
18. Tsai RY, Lenz RK (1989) A new technique for fully autonomous and efficient 3D roboticshand/eye calibration. IEEE Trans Robot Autom 5(3):345–358
19. Wang CM (1988) Location estimation and uncertainty analysis for mobile robots. In: 1988 IEEE international conference on robotics and automation, Philadelphia, PA, pp 1230–1235